FEATURE ARTICLE

Hydrophobicity at Small and Large Length Scales

Ka Lum,[†] David Chandler,*[,†] and John D. Weeks[†,‡]

Department of Chemistry, University of California, Berkeley, California 94720, and Institute for Physical Science and Technology and Department of Chemistry, University of Maryland, College Park, Maryland 20742

Received: November 6, 1998

We develop a unified and generally applicable theory of solvation of small and large apolar species in water. In the former, hydrogen bonding of water is hindered yet persists near the solutes. In the latter, hydrogen bonding is depleted, leading to drying of extended apolar surfaces, large forces of attraction, and hysteresis on mesoscopic length scales. The crossover occurs on nanometer length scales, when the local concentration of apolar units is sufficiently high, or when an apolar surface is sufficiently large. Our theory for the crossover has implications concerning the stability of protein assemblies and protein folding.

Introduction

It has long been accepted that hydrophobic interactions—the effective attractions between apolar groups in water—play a central role in the stability of mesoscopic assembly and biological structure in aqueous environments.[1,2] Yet, a quantitative understanding of this role has been elusive. One obstacle to this understanding is the multifaceted nature of hydrophobic interactions that we focus upon in this paper. In particular, we show how hydrophobic interactions between small apolar groups at low concentrations in water are very different from those between large assemblies or relatively high concentrations of hydrophobic groups in water. The former is pertinent when considering, say, the aqueous solvation of a butane or butanol molecule. The latter is relevant to the solvation of macromolecules such as proteins. In this paper, we present a quantitative theory for these two regimes and show that the crossover between them occurs on nanometer length scales.

Figure 1 juxtaposes hydrophobicity on small and large length scales. Hydrophobic units do not hydrogen bond to water and create excluded volume regions where the density of water molecules vanishes. When these units are small enough, water can reorganize near them without sacrificing hydrogen bonds. The entropic cost of this structural change leads to low solubility for small apolar species in water. The cost and corresponding solubility are readily understood and computed in terms of properties of homogeneous bulk water, such as its radial distribution function.[3−6] There is, however, no strong inducement for small numbers of small hydrophobic groups to associate in water. It is more likely that water will separate such species rather than drive them together.[4,6,7]

On the other hand, close to a large hydrophobic object, perhaps an assembly of several apolar units possibly interspersed with a few hydrophilic units, the persistence of a hydrogen bond network is geometrically impossible. The resulting energetic

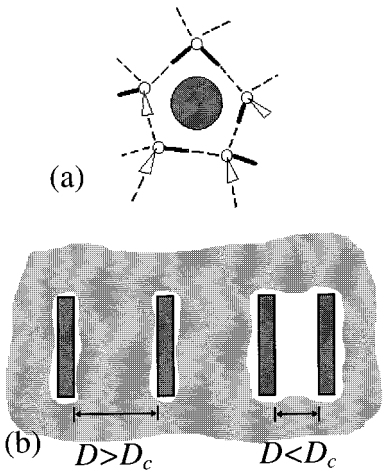

Figure 1. (a) Schematic view of local water structure near a small hydrophobic sphere. Dashed lines indicate hydrogen bonds. (b) Schematic view of water structure near large parallel hydrophobic plates. Shaded area indicates regions where water density is essentially that of the bulk liquid; vacant regions indicate where water density is essentially that of the bulk vapor.

effect can induce drying, as envisioned by Stillinger.[3] Further, this drying can lead to strong attractions between large hydrophobic objects, as observed in surface force measurements.[8] For example, the loss of hydrogen bonds near the two extended hydrophobic surfaces depicted in Figure 1b causes water to move away from those surfaces, producing thin vapor layers. Fluctuations in the interfaces formed in this way can destabilize and expel the remaining liquid contained between these surfaces. The resulting pressure imbalance will cause the surfaces to attract. If the liquid is close to coexistence with the vapor phase, as is the case for water at ambient conditions, this phenomenon occurs with widely separated surfaces.

For the geometry pictured in Figure 1b, macroscopic considerations provide an estimate of when the intersurface separation, D, is sufficiently small for this destabilization to occur. The bounded liquid has an unfavorable surface energy propor-

[†] University of California.
[‡] University of Maryland.

10.1021/jp984327m CCC: $18.00
Published on Web 04/16/1999

tional to the net surface area, where the surface tension, γ, is the constant of proportionality. This energy is counteracted by the favorable bulk free energy proportional to the average number of molecules in the bounded liquid, where the proportionality constant is the difference between liquid and gas chemical potential, $\mu_l - \mu_g$. For large enough D, provided $\mu_l - \mu_g < 0$, the bulk energy dominates over the surface energy, and the bounded liquid is stable. On the other hand, when D is less than the critical separation

$$D_c \approx \frac{2\gamma}{n_l|\mu_l - \mu_g|} \tag{1}$$

surface energy is dominant and the bounded liquid is destabilized with respect to the vapor. Here, n_l is the molecular density of the bulk liquid (the average number of molecules per unit volume). Accordingly, for water at room temperature and atmospheric pressure,[9] $D_c \approx 100$ nm. At this large length scale, the evaporation of water induced by drying surfaces would seem to be a generic and well understood phenomenon,[10−12] and its pertinence to hydrophobicity at large length scales has not gone without attention.[13−16] However, since drying is a nonlinear phenomenon, its manifestation at large length scales is affected by small length scale structure. Self-consistency between small and large length scale effects is missing in these earlier treatments.

Depletion of water near extended hydrophobic surfaces was not observed in early computer simulation studies because the large density fluctuations that would produce it could not be generated in these calculations.[17−19] Recently, however, Wallqvist and Berne[20] succeeded in observing the phenomenon by simulating nanometer sized hydrophobic units contained within a significantly larger constant-pressure bath of water. Thus, it is clear that experimental probes of hydrophobicity on small length scales (such as measuring relative solubilities of alkanes in water) determine something very different from those that probe on large length scales (as done in surface force experiments). Further, Wallqvist and Berne's work[20] suggests that the crossover (or size of the critical nucleus where oil and water might separate) is on the scale of nanometers. Thus, neither extreme of a small length scale or a large length scale description is by itself sufficient to apply to biological assembly. A satisfactory treatment of hydrophobicity must describe both regimes simultaneously.

In this paper, we provide such a treatment. We do so in a way that applies rather generally, not just to water with hydrophobic solutes. The theory first focuses on a component of the fluid density that varies slowly in space. This component sustains interfaces, liquid−vapor phase equilibria, and drying and can be determined very generally in terms of only a few macroscopic parameters like the surface tension. The molecular scale detail that distinguishes the local structure of one liquid from another enters the theory explicitly in a second step, where the effects of small length scale fluctuations about the slowly varying component are estimated. This step takes proper account of excluded volume regions where the density vanishes.

This two-step treatment has been developed in detail from a rigorous statistical mechanics perspective by Weeks, Katsov, and Vollmayr[21] for the special case of a simple fluid interacting with a pair potential. Here, we describe a more heuristic but qualitatively accurate method that can be applied more generally, in particular to water. The result of this analysis is a theory with mathematical similarities to dielectric continuum theory. It reduces to Pratt−Chandler theory[4,6] for small apolar units but crosses over to something very different when hydrophobic surfaces extend over a nanometer.

Theory

The fluctuating molecular density field $\rho(\mathbf{r})$ at position $\mathbf{r}$, with average value $\langle\rho(\mathbf{r})\rangle \equiv n(\mathbf{r})$, provides a convenient measure of the microscopic configurations. This field gives the local concentration of centers of water molecules. (For the purposes of specificity, the "center" can be, for example, the position of the oxygen nucleus.) Since water is a fluid of polyatomic molecules, a complete description of its instantaneous structure requires more than just this scalar quantity. The primary effect of hydrophobic units in water, however, is to expel water molecules from the regions occupied by those units. Once the consequences of this expulsion are understood, other effects, such as those due to solute−solvent attractions, can be treated either as first order perturbations[4,22−24] or by mean field theory,[21] as described below. Thus, in this paper our primary focus is on estimating the free energy cost or reversible work to make $\rho(\mathbf{r}) = 0$ for $\mathbf{r}$ in a hydrophobic volume v. With this focus, other details about local water structure play no explicit role. Orientational structure appears only implicitly in the way it influences the statistics of $\rho(\mathbf{r})$. It is a remarkable fact that over small length scales this statistics is essentially Gaussian,[5,6] a fact we make use of shortly.

For the homogeneous fluid, $n(\mathbf{r})$ is simply the constant bulk density, n_l. Excluded volume, however, creates gradients in the average density $n(\mathbf{r})$ and in many cases can induce rapidly varying components analogous to the oscillations in the fluid radial distribution function, manifesting molecular scale granularity of the liquid.[25] Since molecules in the liquid attract one another with some finite range of interaction, λ, any such spatial variation of $n(\mathbf{r})$ must be accompanied by a gradient in the energy density field arising from the attractive intermolecular interactions. This produces a net force from the unbalanced attractive interactions directed towards the region of higher density.[26] The attractive energy density field can be written as $-2a\bar{n}(\mathbf{r})$, where the overbar indicates a normalized average or coarse graining of the fluid density $n(\mathbf{r})$ over the length scale λ and $-n^2a$ is the adhesive energy density of the homogeneous fluid of density n.[27] We will see that, for water, $\lambda \approx 0.3$ nm. Averaging over the length scale of attractive interactions smooths out quickly varying oscillatory components of $n(\mathbf{r})$. Thus, the resulting $\bar{n}(\mathbf{r})$ is relatively slowly varying, even when $n(\mathbf{r})$ itself might be rapidly varying. We call $\bar{n}(\mathbf{r})$ the coarse grained density and will exploit its relatively slow variation in our calculation of the full $n(\mathbf{r})$.

To that end, let us first recall the usual square gradient theory for a slowly varying free liquid−vapor interface.[10,28] This theory applies only when the density field varies little over the length scale λ. In that case, the statistical weight for a given $\rho(\mathbf{r})$ in the grand canonical ensemble is proportional to $\exp\{-\beta F_0[\rho(\mathbf{r})]\}$, where $F_0[\rho(\mathbf{r})]$ is the effective Hamiltonian or free energy functional

$$F_0[\rho(\mathbf{r})] = \int d\mathbf{r}\left[w(\rho(\mathbf{r})) + \frac{1}{2}m\left|\nabla\rho(\mathbf{r})\right|^2\right] \tag{2}$$

Here, $\beta^{-1} = k_B T$ is Boltzmann's constant times temperature, $w(\rho(\mathbf{r})) = w(\rho(\mathbf{r});\mu)$ is a local free energy density parameterized by the ambient chemical potential μ, and $m = a\lambda^2$.[29] [The subscript "0" indicates the absence of any imposed excluded volume that would induce rapid spatial variation in $\rho(\mathbf{r})$.]

In mean field theory, the equilibrium $n(\mathbf{r}) = \langle\rho(\mathbf{r})\rangle$ is the function that minimizes this free energy, i.e., $0 = \delta F_0/\delta n(\mathbf{r})$.

This condition yields the well known differential equation for $n(\mathbf{r})$[28]

$$w'(n(\mathbf{r})) = m\nabla^2 n(\mathbf{r}) = 2a[\bar{n}(\mathbf{r}) - n(\mathbf{r})] \quad (3)$$

where $w'(n) = \partial w/\partial n$. At phase equilibrium, where a liquid of homogeneous density n_l coexists with a gas of homogeneous density n_g, the conditions of constant pressure and chemical potential correspond to $w(n_l) = w(n_g)$ and $w'(n_l) = w'(n_g) = 0$, respectively. Under these conditions, there exists a slowly varying solution to eq 3 describing the liquid−vapor interface. In the second line of eq 3, the Laplacian term has been rewritten in terms of the coarse grained density $\bar{n}(\mathbf{r})$; the expressions are equivalent by second order Taylor expansion of $n(\mathbf{r}')$ about $n(\mathbf{r})$in the integration that defines the coarse grained density. [See, for example, eq 14 below.]

In general, however, excluded volume regions or other perturbations can induce rapidly varying components in $n(\mathbf{r})$ that cannot be described by eqs 2 and 3. Nevertheless, even in such cases, the associated coarse grained density, $\bar{n}(\mathbf{r})$, remains slowly varying. This observation allows us to determine a slowly varying component of the full density.[21] The rapidly varying component will be treated in a second step as discussed below and the self-consistent combination of both components will give an accurate description of the full $n(\mathbf{r})$.

We denote the slowly varying component by $n_s(\mathbf{r})$ and require that it satisfy eq 3 when the coarse grained density arising from the full *n(r)* is used:

$$w'(n_s(\mathbf{r})) = 2a[\bar{n}(\mathbf{r}) - n_s(\mathbf{r})] \quad (4)$$

The relation to the usual free interface theory becomes clearer if we add and subtract the coarse grained density of the slowly varying component, $\bar{n}_s(\mathbf{r})$, and expand as before. This yields our final result,

$$w'(n_s(\mathbf{r})) = m\nabla^2 n_s(\mathbf{r}) + 2a[\bar{n}(\mathbf{r}) - \bar{n}_s(\mathbf{r})] \quad (5)$$

Equation 5 is the general formula for a slowly varying density field $n_s(\mathbf{r})$ in the presence of the (self-consistent) potential, $-2a[\bar{n}(\mathbf{r}) - \bar{n}_s(\mathbf{r})]$. This field takes account of the extra unbalanced attractive energy density arising from the rapidly varying component of the density, $n(\mathbf{r}) - n_s(\mathbf{r})$. In general, $n_s(\mathbf{r})$ contains most of the long-wavelength variation of the full density, and in the absence of rapid spatial variation of the density, $n(\mathbf{r}) = n_s(\mathbf{r})$. In that case, eq 5 reduces to the standard theory for slowly varying inhomogeneous density fields, eq 3. The theory is altered, however, by the presence of rapidly varying components in $n(\mathbf{r})$, such as those induced by excluded volume. The last term in eq 5 is then not negligible. This term permits interface-like solutions for $n_s(\mathbf{r})$ over a continuous range of temperature and density. Without it, spatially varying solutions exist only at liquid−gas coexistence, where $w(n)$ has two equal minima located at the coexisting liquid and gas densities.

The small length scale differences between $n_s(\mathbf{r})$ and the full density field $n(\mathbf{r})$ are determined in a second step by averaging $\delta\rho(\mathbf{r}) = \rho(\mathbf{r}) - n_s(\mathbf{r})$, taking proper account of excluded volume regions. To the extent that $\delta\rho(\mathbf{r})$ is a Gaussian random field, the method for carrying out such an average is well known.[5] Moreover, Hummer et al.[6] have established that small length scale density fluctuations in water are indeed Gaussian. With such statistics, we find that $n(\mathbf{r})$ is given by

$$n(\mathbf{r}) = \langle\rho(\mathbf{r})\rangle_\upsilon = n_s(\mathbf{r}) - \int d\mathbf{r}' c(\mathbf{r}')\,\chi(\mathbf{r}', \mathbf{r}) \quad (6)$$

where angled brackets labeled with the subscript "υ" indicate the presence of the solute excluding solvent from the volume υ. The function

$$\chi(\mathbf{r}, \mathbf{r}') = \langle\delta\rho(\mathbf{r})\,\delta\rho(\mathbf{r}')\rangle_0 \quad (7)$$

is the variance for the Gaussian statistics with a specified $n_s(\mathbf{r})$, but in the absence of the solute (or any other source of inhomogeneities that vary quickly in space). The function $c(\mathbf{r})$ is nonzero only for $\mathbf{r}$ contained in the excluded volume υ, and in that region, $c(\mathbf{r})$ is determined by the requirement that $n(\mathbf{r}) = 0$ for all $\mathbf{r}$ in υ. [30] Equation 6 is a generalization of eq 2.8 of ref 5. For the case of long length scale homogeneity, i.e., when $n_s(\mathbf{r}) = n$, eq 6 is the Pratt−Chandler integral equation for the distribution function of water surrounding an apolar solute.[4] This occurrence of homogeneity is obtained from eq 5 when the hydrophobic solute (i.e., when the excluded volume) is relatively small.

Equations 5 and 6 provide a self-consistent theory for water density near hydrophobic solutes.[31] In addition to this structural property, free energies of solvation are also of interest. For ideal hydrophobic units, i.e., species that simply exclude water from specified volumes, solvation free energies are related to the probability of finding these volumes empty in the unperturbed fluid.[6] Such a probability is a ratio of partition functions. Specifically, the excess chemical potential for a hydrophobic object excluding the volume υ is

$$\Delta\mu_\upsilon = -k_B T \ln\left[\frac{Z_\upsilon(0)}{\sum_{N\geq 0} Z_\upsilon(N)}\right] \quad (8)$$

where $Z_\upsilon(N)$ is the partition function when N solvent molecules occupy the volume υ. Using Gaussian statistics to estimate the probability, we find that this partition function is given by[32]

$$Z_\upsilon(N) = \exp\{-F_0[n_s(\mathbf{r};N)]/k_B T - [N - \int_\upsilon d\mathbf{r}\, n_s(\mathbf{r};N)]^2/2\sigma_\upsilon - (\ln \sigma_\upsilon)/2\} \quad (9)$$

where

$$\sigma_\upsilon = \int_\upsilon d\mathbf{r} \int_\upsilon d\mathbf{r}'\, \chi(\mathbf{r},\mathbf{r}') \quad (10)$$

In these relationships, the integrals labeled with a subscript "υ" are over the excluded volume υ, and $n_s(\mathbf{r};N)$ is computed from eq 5, but eq 6 is replaced by

$$n(\mathbf{r};N) = n_s(\mathbf{r};N) - \int_\upsilon d\mathbf{r}' \int_\upsilon d\mathbf{r}''[n_s(\mathbf{r}';N) - N/\upsilon]\sigma_\upsilon^{-1}\,\chi(\mathbf{r}'',\mathbf{r}) \quad (11)$$

In the limit of small excluded volumes, eq 11 will predict a small unbalanced force, and the resulting $n_s(\mathbf{r};N)$ will be close to the bulk liquid density, n_l. In that case, eqs 9 and 10 reduce to the free energy of hydrophobic hydration developed and used by Hummer et al. to successfully interpret the solvation of small apolar species in water.[6,24] In general, however, the main physical effect of the unbalanced attractive forces taken into account in the first step of our method is to reduce the density

near the excluded volume region, thus permitting a lower solvation free energy.

Applications

The theory presented above is a relatively general treatment of solvation excluded volume effects. To characterize the long-wavelength properties of the water solvent determined in the first step of our theory, we must give a prescription for carrying out the coarse graining implied by the overbars in eq 5 and values for $w(n)$ and m. Since this step is essentially independent of the local structure, any reasonable form of these quantities is sufficient provided it is fit to the macroscopic properties of water over the thermodynamic range of interest. Therefore, we adopt the simplest possible van der Waals forms[28]

$$w(n) = nk_BT\ln\left(\frac{bn}{1-bn}\right) - an^2 - \mu n \qquad (12)$$

When the chemical potential μ is such that liquid and gas coexist,

$$\gamma = \int_{n_g}^{n_l} dn\sqrt{2m[w(n) - w(n_g)]} \qquad (13)$$

where n_g and n_l are the bulk gas and liquid densities, respectively, at the liquid−gas coexistence implied by $w(n)$. We fit the molecular volume parameter, b, and the energy density parameter, a, so that (i) n_l has the value of the liquid water's density at phase coexistence when $T = 298$ K and (ii) the compressibility implied by $w(n)$ has the same value as that for water at normal conditions. These conditions yield $a \approx 230$ kJ cm^3/mol^2 and $b \approx 15$ cm^3/mol. Then, with surface tension given by that for liquid water at normal conditions, i.e., $\gamma \approx 72$ mJ/m^2 $\approx 18\ k_BT$/nm^2, the second van der Waals relation gives $\lambda^2 \equiv m/a \approx (0.38\text{ nm})^2$. Finally, for the coarse graining prescription, we use a simple Gaussian weight

$$\bar{n}(\mathbf{r}) = \int d\mathbf{r}'n(\mathbf{r}')\,(2\lambda^2\pi)^{-3/2}\exp(-|\mathbf{r}-\mathbf{r}'|^2/2\lambda^2) \qquad (14)$$

The unique local structure of water enters explicitly in the second step of our theory through the specification of $\chi(\mathbf{r},\mathbf{r}')$ in eq 6. Here too we use experimental data, setting

$$\chi(\mathbf{r},\mathbf{r}') \simeq n_s(\mathbf{r})\,\delta(\mathbf{r}-\mathbf{r}') + n_s(\mathbf{r})\,n_s(\mathbf{r}')\,h(|\mathbf{r}-\mathbf{r}'|) \qquad (15)$$

where $h(|\mathbf{r}-\mathbf{r}'|) + 1$ is the radial distribution function of liquid water at the bulk density n_l.[33] Approximation 15 becomes exact in the limit of homogeneity, $n_s(\mathbf{r}) = n_l$, and in the limit of low density. It is well-defined at intermediate densities and serves as a computationally practical interpolation formula.

Our choices for these quantities are rather arbitrary but still consistent with the most important physical aspects of hydrophobicity. For instance, to correctly predict the onset of drying, it is important that the proximity of liquid−gas coexistence is accurately represented. To correctly estimate $\chi(\mathbf{r},\mathbf{r}')$ in the drying regime where density is low, it is also important that this function is consistent with the exact low-density form, $n_s(\mathbf{r})\,\delta(\mathbf{r}-\mathbf{r}')$. When drying does not occur and short length scale effects dominate, it is important that $\chi(\mathbf{r},\mathbf{r}')$ is consistent with the exact form for the homogeneous liquid, $n_l\delta(\mathbf{r}-\mathbf{r}') + n_l^2\,h(|\mathbf{r}-\mathbf{r}'|)$. All these features are captured by our choices, and other details have relatively small effects on numerical results derived from the theory. For example, in the applications reported below, no qualitative changes are found on altering the value of γ by 20%, or on altering the coarse graining prescription, eq 14, to some other reasonable choices. An equation of state more accurate than (12) might help in making predictions over a wide range of temperatures, but for the use we make of it here, eq 12 seems satisfactory.

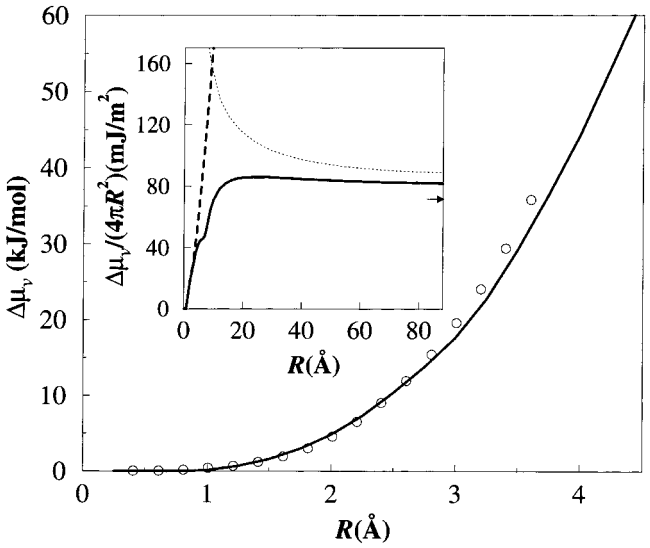

Figure 2. Excess chemical potential for a hard sphere of radius R in water. The solid lines indicate the results of eqs 5, 9, and 11. The circles are the results of computer simulations.[6] The dashed line is the result of the Gaussian model, namely eq 9 with $n_s(r) = n_l$.[6] The dotted line is a continuum theory estimate (see text for description). The arrow indicates the value for the surface tension of water.

With these ingredients in hand, we have carried out a series of calculations to illustrate the predictions of the self-consistent structural eqs 5 and 6 and the corresponding free energy relations (9) and (11).

Hydration of Hard Spheres. Our first application concerns the hydration of a hard sphere excluding water from a volume of radius R centered at the origin. Figure 2 shows the excess chemical potential, $\Delta\mu_v$, as a function of R computed from the theory. In the field of structural biology, it is often assumed that hydrophobic solvation energies are proportional to exposed hydrophobic surface area.[34−36] As such, one might expect that $\Delta\mu_v$ would be proportional to R^2. For $R \gtrsim 2$ nm, the theory shows that the ratio $\Delta\mu_v/4\pi R^2$ does reach an approximate plateau with a value similar to that of the surface tension, γ. For smaller R, however, $\Delta\mu_v/4\pi R^2$ is a rapidly varying function of R. This variability explains why there is no consensus over the appropriate hydrophobic energy per unit area governing nanometer assemblies, such as protein structures. On a nanometer length scale, there is no unique value.

For small spheres ($R < 0.4$ nm), $\Delta\mu_v$ has been estimated by computer simulation.[37] Figure 2 shows that theory is in good accord with the simulation results. In this small-sphere regime, the full theory also differs little from the predictions of simple Gaussian statistics, namely eq 9 with $n_s(\mathbf{r};N) = n_l$. Gaussian statistics is the basis for the Pratt−Chandler theory of hydrophobicity,[5] both in its traditional form[4] and its recent extension.[6] The agreement between theory and simulation in this regime is consistent with the successes of that theory in predicting, for example, free energies of transfer and solubilities of small hydrophobic molecules. For $R \gtrsim 1$ nm, however, the predictions of the Gaussian model diverge from those of the full theory. The divergence is due to drying. This phenomenon is predicted by the full theory, but it is outside the scope of the Gaussian model. In view of the disparity, it may be inappropriate to use the Gaussian model to interpret temperature and pressure effects on the stability of protein structures.[24]

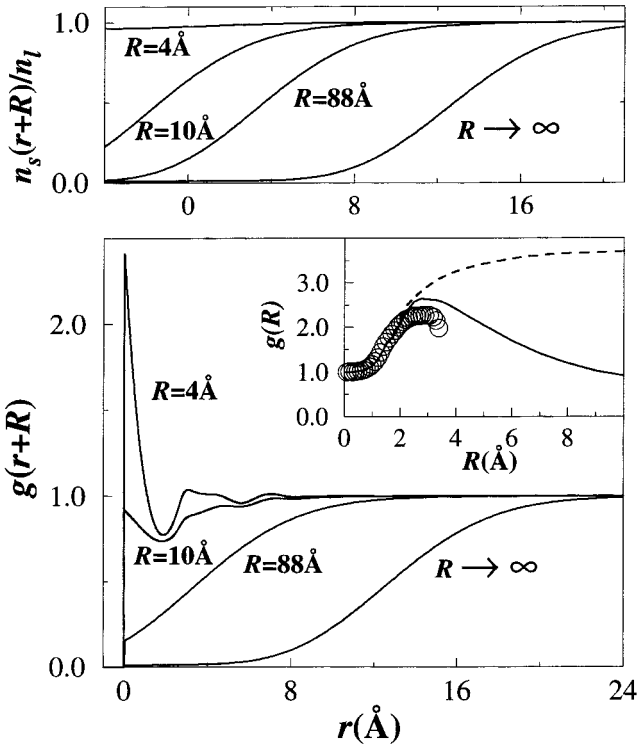

Figure 3. (upper part) Slowly varying component $n_s(R + r)$ of the average water density as a function of the distance $R + r$ from the center of excluded volume regions with varying radii R. (lower part) Radial distribution function $g(R + r) \equiv n(R + r)/n_l$ giving the net average water density around the same excluded volume regions. The inset graph focuses on the contact value of that function. Solid lines are the results of eqs 5 and 6. Circles are the results of computer simulations.[37] The dashed line is from the Gaussian model, namely eq 6 with $n_s(r) = n_l$.[4]

For large R, one might consider employing a simplified continuum theory based upon eq 5, but replacing the self-consistent field term with boundary conditions $n_s(\mathbf{r};N) = N/v$ for $r \leq R$ and $n_s(\mathbf{r};N) = n_l$ for $R \rightarrow \infty$. In general, the $n_s(\mathbf{r};N)$ constructed in this way will vary rapidly near the surface of the volume v. This continuum theory is therefore not self-consistent. Moreover, eq 5 shows that the self-consistent field is nonzero outside the surface and cannot be represented by a single boundary condition. Indeed, the predictions of the continuum model are unsatisfactory in the physically interesting cross-over regime, as shown in Figure 2.

The solute−water radial distribution function, $g(r + R) = n(r + R)/n_l$, as a function of the distance $r + R$ from the center of an excluded volume region of radius R, directly illustrates the nature of the drying phenomenon. This function is shown in Figure 3. For small spheres, $g(r + R)$ exhibits oscillations manifesting the microscopic granularity of liquid water. For $R \gtrsim 1$ nm, density depletion is evident and the magnitude of the oscillations decreases. For large R, $g(r + R)$ rises smoothly with increasing r. Evidently, a ball of oily groups with radius larger than 1 nm, e.g., a spherical cluster of about 20 methyl groups, is large enough to induce drying. Significantly smaller assemblies will not induce this effect.

The behavior of $n(\mathbf{r})$ for water near a large hard sphere is thus much like that for the liquid near a free liquid−gas interface, as Stillinger envisioned long ago.[3] Stillinger also theorized that the contact value, i.e., $g(R)$, is a nonmonotonic function of R. For small R, the removal of water within the excluded volume is accommodated by an increase in density adjacent to the volume. For small R, $g(R)$ is therefore an increasing function of R. For large enough R, however, drying sets in, making $g(R)$ a decreasing function of R. Stillinger made numerical predictions of this behavior, based upon an algebraic interpolation formula connecting two regimes of small and large hydrophobic spheres. His predictions agree qualitatively with the results of our theory shown in Figure 3. These theoretical results also agree reasonably well with computer simulation results, over the limited regime where these simulation results are available. Better agreement would probably require better estimates of $w(n)$ and $\chi(\mathbf{r},\mathbf{r}')$ than those we have used as input for the calculations.

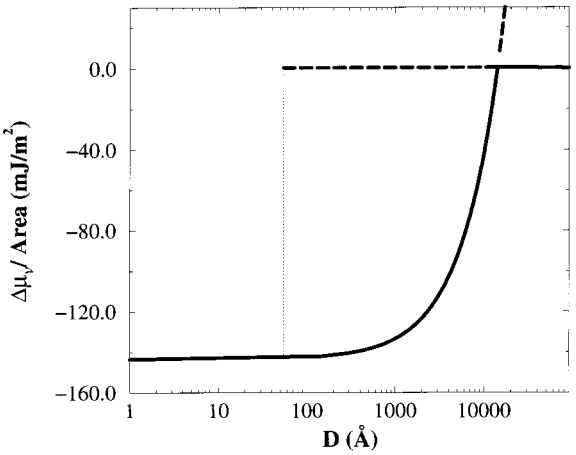

Figure 4. Free energy per unit surface area for water confined between two parallel hard surfaces separated a distance D. The zero of free energy is taken as the $D \rightarrow \infty$ limiting value. The curves are computed from eqs 5, 9, and 11, with $N = 0$. Solid lines refer to stable branches, dashed lines refer to metastable branches, and the dotted line shows the small D limit of stability for the liquid density phase.

Hydration of Two Parallel Hard Plates. As discussed in the Introduction, drying of extended hydrophobic surfaces can lead to strong attractions between pairs of such surfaces. As a second application, we therefore consider the solvent-induced interactions between a pair of two infinite hard plates. The plates lie parallel to the $x - y$ axis of a Cartesian coordinate system, and they exclude water from the regions $z < 0$ and $z > D$. With this arrangement, our calculations provide an interpretation of surface force measurements. These experiments reveal long ranged forces between hydrophobic surfaces in water. While disagreeing over quantitative details,[8] they show that an attractive force becomes measurable at large intersurface separation, in most cases up to tens of nanometers. Further, when brought to separations of about 10 nm, two hydrated parallel hydrophobic plates will jump into contact. Hysteresis is observed in the inward- and the outward-going measurements, indicative of a kinetically frustrated first order phase transition.

Hysteresis is predicted by our analysis in that over a range of D values, there are two solutions to eq 5 and thus two different free energies. The resulting free energy branches as a functions of D are shown in Figure 4. In agreement with the elementary estimate, eq 1, the figure shows that even for relatively large interplate separations, the confined liquid water is less thermodynamically stable than its vapor. The liquid remains metastable over a wide range of D. In this regime, the kinetic pathway to evaporation involves fluctuations of the water interfaces sufficient to create a vapor bridge between the two plates.[16,38] Such large fluctuations occur only rarely. To a good approximation, water will remain between the plates until D is made so small that the confined liquid becomes mechanically unstable. Figure 4 shows that this limit of metastability (i.e., the spinodal) of confined water is reached when $D \approx 5$ nm.

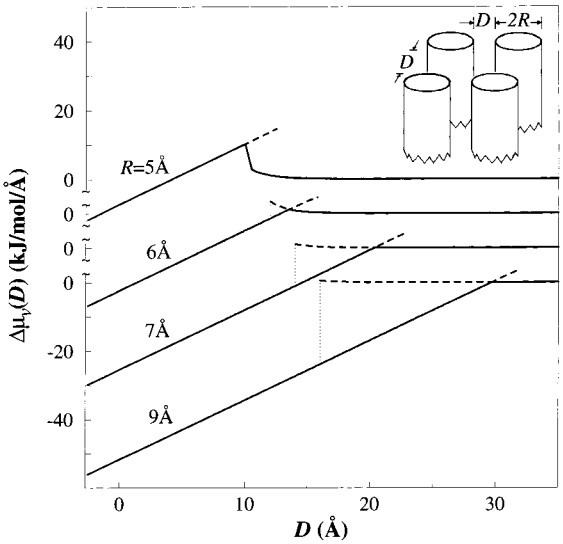

Figure 5. Free energies per unit length for water interacting with four parallel hard cylinders (pictured at top). The distance of closest approach between cylinders is taken as $D = -0.27$ nm. The zero of free energy is taken as the $D \rightarrow \infty$ limiting value. Curves are computed from eqs 5, 9, and 11. Solid lines refer to stable branches, dashed lines refer to metastable branches, dotted lines refer to small-D limits of stability for the high-density solutions. The limits of stability of the low-density solution are off the scale of this figure.

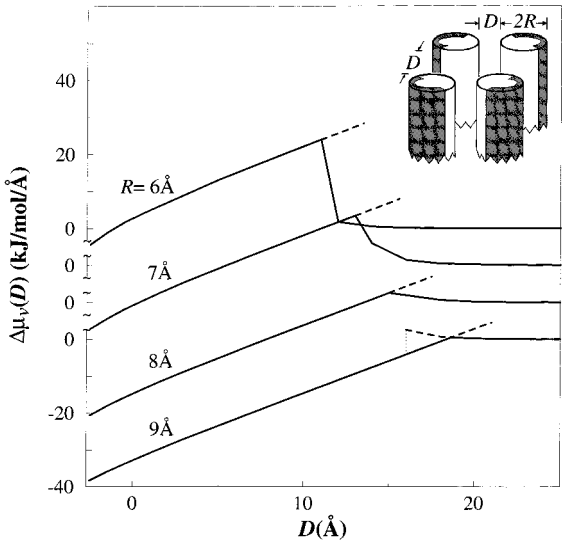

Figure 6. Free energies per unit length for water interacting with four parallel hard cylinders with hydrophilic outer sides. The parallel cylinders are depicted at the top of the figure; the shaded area denotes the hydrophilic regions. The distance of closest approach between cylinders is taken as $D = -0.27$ nm. The zero of free energy is taken as the $D \rightarrow \infty$ limiting value. Curves are computed from eqs 9 and 11 and eq 5 modified by subtracting the field $\phi(\mathbf{r})$ from its right-hand side. Solid lines refer to stable branches, the dashed line refers to the metastable branch, and the dotted line refers to the small-D limit of stability for the high-density solutions. The limits of stability of the low-density solution are off the scale of this figure.

This length is comparable to the distance where hydrated hydrophobic surfaces jump into contact in surface force experiments. According to our theory, this jump distance will decrease as the bulk liquid moves away from phase coexistence, for example, by decreasing temperature or adding salt to the liquid. Further, the jump distance will increase with the addition of kinetic pathways to evaporation, such as the presence of gas bubbles in the solvent.

Since mean field theory is used to describe large length scale structure, capillary waves are not included in our treatment. These small-amplitude interfacial fluctuations adjacent to each plate surface give rise to weak long-range interplate attractions. A complete theory for large-distance attractions between extended hydrophobic surfaces must account for this capillary wave effect. Such long ranged forces, however, are relatively small in comparison with the those produced by drying and evaporation.

Hydration of Parallel Cylinders. An array of four parallel cylinders provides another instructive application, evocative of helix bundle motifs common in protein structures.[39] Specifically, we have carried out calculations of water densities and free energies in the presence of four infinite cylinders, each of radius R, where the axis of each cylinder is parallel to the z axis of a Cartesian coordinate system. These axes form a square in the $x-y$ plane with side length $D + 2R$. Thus, water is expelled from the regions $[x \pm (R + D/2)]^2 + [y \pm (R + D/2)]^2 < R^2$.

For this geometry of hydrophobic units, the computed excess chemical potentials per unit length are shown in Figure 5 as a function of surface-to-surface separation, D. For cylinders with $R \gtrsim 0.6$ nm, there is a range of D values where metastable high-density states are found. For smaller cylinders, there is no such metastability. For all cases illustrated, the low-density phase is stable for $D \lesssim 1$ nm, and the stability or metastability of this phase creates a powerful force favoring the assembly of the four cylinders. For $R \gtrsim 0.7$ nm, the free energy barrier to association disappears, even in the metastable branch. For this regime, one therefore expects both powerful and relatively rapid association of the hydrophobic units. Conversion to net free energies requires multiplication of $\Delta\mu_v$, per unit length by the actual length for the cylinders. Thus, features illustrated in Figure 5 reveal net free energetic effects that can be very large compared to k_BT.

Figure 5 projects onto only one coordinate, D. The absence of a free energy barrier to association in that direction does not necessarily imply the actual pathway to association is barrier free. The actual pathway can have dynamical bottlenecks involving water density fluctuations such as described above for the case of two parallel plates.

For all cylinders considered in Figure 5, mean field theory predicts the low-density phase remains metastable for $D \gtrsim 10$ nm. In this phase, the four cylinders are encapsulated by a vapor bubble of similar shape. Density fluctuations, i.e., thermal excursions of the liquid−vapor interface, will break the bubble at values of D smaller that those of the mean field stability limits.

Surfaces of helices assembling in actual protein structures are not entirely hydrophobic. The trends illustrated in Figure 5, however, depend mostly on the fact that the interior surfaces of the assembled bundle are hydrophobic. To show this fact, we have considered modified parallel cylinders, where the outer halves of the cylinders are hydrophilic, as illustrated in the upper part of Figure 6. In particular, we have carried out calculations with eq 5 modified by subtracting an attractive interaction $\phi(\mathbf{r})$ from its right-hand side, where

$$\phi(\mathbf{r}) = -2an_1 \int d\mathbf{r}'\alpha(\mathbf{r}')\,(2\lambda^2\pi)^{-3/2} \exp(-|\mathbf{r} - \mathbf{r}'|^2/2\lambda^2) \tag{16}$$

and $\alpha(\mathbf{r})$ is unity for $\mathbf{r} \in v'$ and zero otherwise. Here, v' refers to a hydrophilic shell that coats the outer half surface of each cylinder and extends 0.3 nm within. Other choices for the strength and functional form of this potential field are possible. The basic idea is to create a water-like region within the solute.

With eq 16, it is as if a layer of water molecules of density n_l lies inside the outer-half surface of each cylinder.

Results obtained with this modification of eq 5 are plotted in Figure 6. While details differ, the trends obtained for fully hydrophobic cylinders are indeed similar to those obtained with partially hydrophobic cylinders. For example, the size of free energy barriers are larger in the latter than in the former, and the radius required for high-density metastable branches to appear is larger in the latter than in the former.

Implications

Mesoscopic structures are stabilized by a variety of forces. To the extent that hydrophobic forces are significant, this paper illuminates a number of important facts. First and foremost, hydrophobic effects of the type that separate oily groups from aqueous solution appear only when local concentrations of hydrophobic units are large enough or extended enough to induce drying. Excess chemical potentials and transfer free energies of single small apolar species, like alkane chains of moderate length, reveal nothing of the powerful interactions created by drying. Similarly, the structure of water near small apolar species provides little or no hint of the phenomenon that inevitably dominates for larger hydrophobic assemblies.

Even in the presence of hydrophilic surfaces, powerful hyrophobic forces of assembly can arise from drying transitions. To the extent that these forces are relevant to biological assembly, one can anticipate general trends affecting the stability of such structures. Specifically, changes in solvent that move the bulk liquid away from liquid−gas phase coexistence (e.g., adding salt, increasing pressure, lowering temperature) will shorten the range and weaken these forces of assembly.

Since powerful hydrophobic interactions require the onset of a phase transition, the dynamics of assemblies stabilized by this interaction will depend, at least in part, on the dynamics of the phase transition. Thus, for example, aspects of water structure and drying may play a significant role in the kinetic pathways to protein folding for transitions between configurations of differing hydrophobic stabilization. This possibility would explain directions of trends observed in the binding−unbinding kinetics of helix pairs in Rop.[40] Indeed, the evaporation kinetics of water confined by hydrophobic surfaces is significantly slowed by adding a low concentration of hydrophilic spots to the surfaces[41] since water interfaces are pinned at these spots. Most standard models of protein folding include water only implicitly, through its effect on free energy surfaces, and assume that water is continually at equilibrium with the assembling solutes. We believe that water plays a more explicit role in the dynamics than can be captured with such implicit equilibrium models.

Drying is a collective phenomenon. As such, pair potentials of mean force between small apolar units are insufficient for characterizing its onset. The onset or crossover to drying is found at the nanometer regime, the length scale of pertinence to protein assembly. In this regime, the phenomenon is too complex to be characterized by a single microscopic parameter, such as exposed surface area. It seems likely, therefore, that most models used thus far in theoretical studies of protein structure oversimplify the true nature of the hydrophobic interactions conceived of long ago by Kauzmann. In contrast, the equations written in this paper could be used to provide a computationally convenient yet accurate means to describe this nature.

Acknowledgment. We are grateful to Lawrence Pratt, Gerhard Hummer, and their co-workers for many helpful discussions and informative preprints about their work on hydrophobicity, to Martin Karplus for telling us about ref 40, and to Kirill Katsov for helpful discussions about the present formalism. This research has been supported by grants from the National Science Foundation (CHE9508336 and CHE9528915).

References and Notes

(1) Kauzmann, W. *Adv. Protein Chem.* **1959**, *14*, 1.

(2) Tanford, C. *The Hydrophobic Effect-Formation of Micelles and Biological Membranes;* Wiley-lnterscience: New York, 1973.

(3) Stillinger, F. H. *J. Solution Chem.* **1973**, *2*,141.

(4) Pratt, L. R.; Chandler, D. *J. Chem. Phys.* **1977**, *67*, 3683.

(5) Chandler, D. *Phys. Rev. E* **1993**, *48*, 2898.

(6) Hummer, G.; Garde, S.; García, A. E.; Pohorille, A.; Pratt, L. R. *Proc. Natl. Acad. Sci. U.S.A.* **1996**, *93*, 8951.

(7) Pangali, C. S.; Rao, M.; Berne, B. J. *J. Chem. Phys.* **1979**, *70*, 2975.

(8) Pashley, R. M.; McGuiggan, P. M.; Ninham, B. W.; Evans, D. F. *Science* **1985**, *229*, 1088. Christenson, H. K.; Claesson, P. M. *Science* **1988**, *239*, 390. Tsao, Y.-H.; Yang, S. X.; Evans, D. F.; Wennerström, H. *Langmuir* **1991**, *7*, 3154. Christenson, H. K. In *Modern Approaches to Wettability: Theory and Applications;* Schrader, M. E., Loeb, G., Eds.; Plenum: New York, 1992. Parker, J. L.; Claesson, P. M.; Attard, P. *J. Phys. Chem.* **1994**, *98*, 8468.

(9) For water at standard conditions of 1 atm and $T = 298$ K, $n_l \simeq 0.055$ mol/cm^3, $\gamma \simeq 72$ mJ/m^2, and $\mu_l - \mu_g \simeq -p/n_l \simeq -1.8$ J/mol, where p denotes pressure. Surface tensions for oil−water interfaces differ only slightly from water-vapor surface tension. The latter is used here. Adopting an oil−water surface tension to estimate D_c would give a similarly large critical intersurface separation. The large value of D_c is primarily a result of the close proximity of phase coexistence (i.e., the relatively small magnitude of $\mu_l - \mu_g$).

(10) Binder, K.; Hohenberg, P. C. *Phys. Rev. B* **1972**, *6*, 3461.

(11) Brézin, E.; Halperin, B. I.; Leibler, S. *J. Phys.* **1983**, *44*, 775.

(12) Parry, A. O.; Evans, R. *Physica A* **1992**, *181*, 250.

(13) Gompper, G.; Hauser, M.; Kornyshev, A. A. *J. Chem. Phys.* **1994**, *101*, 3378.

(14) Bérard, D.; Attard, P.; Patey, G. *N. J. Chem. Phys.* **1993**, *98*, 7236.

(15) Forsman, J.; Jönsson, B.; Woodward, C. E.; Wennerström, H *J. Phys. Chem.* **1997**, *101*, 4253.

(16) Lum, K.; Luzar, A. *Phys. Rev. E* **1997**, *56*, R6283.

(17) Lee, C. Y.; McCammon, J. A.; Rossky, P. J. *J. Chem. Phys.* **1984**, *80*, 4448.

(18) Wallqvist, A.; Berne, B. J. *Chem. Phys. Lett.* **1988**, *145*, 26.

(19) Luzar, A.; Bratko, D.; Blum, L. *J. Chem. Phys* **1987**, *86*, 2955.

(20) Wallqvist, A.; Berne, B. J. *J. Phys. Chem.* **1995**, *99*, 2893.

(21) Weeks, J. D.; Katsov, K.; Vollmayr, K. *Phys. Rev. Lett.* **1998**, *81*, 4400.

(22) Pratt, L. R.; Chandler, D. *J. Chem. Phys.* **1980**, *73*, 3434.

(23) Chandler, D.; Weeks, J. D.; Andersen, H. C. *Science* **1983**, *220*, 787.

(24) Garde, S.; Hummer, G.; García, A. E.; Paulaitis, M. E.; Pratt, L. R. *Phys. Rev. Lett.* **1996**, *77*, 4966. Hummer, G.; Garde, S.; García, A. E.; Paulaitis, M. E.; Pratt, L. R. *Proc. Natl. Acad. Sci. U.S.A.* **1998**, *95*, 1552. Hummer, G., et al. *J. Phys. Chem. B* **1998**, *102*, 10469.

(25) Hansen, J. P.; McDonald, I. *R. Theory of Simple Liquids*; Academic Press: London, 1986.

(26) Weeks, J. D.; Selinger, R. L. B.; Broughton, J. Q. *Phys. Rev. Lett.* **1995**, *75*, 2694.

(27) In the special case of the simple van der Waals fluid, where the attractive forces arise from a relatively long-ranged pair potential $u_l(r)$, the inhomogeneous energy density at position $\mathbf{r}$ is $\int d\mathbf{r}' u_l(|\mathbf{r} - \mathbf{r}'|)n(\mathbf{r}') = -2a\bar{n}(\mathbf{r})$. In this case, $a = -\int d\mathbf{r}' u_l(r)/2$ is the usual van der Waals attractive force parameter. See refs 23 and 28.

(28) Rowlinson, J. S.; Widom, B. *Molecular Theory of Capillarity*; Clarendon Press: Oxford, 1982.

(29) In the special case of the simple van der Waals fluid with pair potential $u_l(r)$, $m/a = \lambda^2 = \int d\mathbf{r} r^2 u_l(r)/3 \int d\mathbf{r} u_l(r)$. See, for example, ref 28.

(30) A numerical solution can be found by adjusting $c(\mathbf{r})$ (perhaps by adjusting its coefficients in a basis set representation) until $n(\mathbf{r}) = 0$ for $\mathbf{r} \in v$ is satisfied to within desired accuracy.

(31) One may make an initial guess for $n_s(\mathbf{r})$, perhaps $n_s(\mathbf{r}) = n_l$, and solve eq 6 with this guess. The resulting $n(\mathbf{r})$ can then used to solve the differential eq 5 for $n_s(\mathbf{r})$, perhaps through a discrete expansion on a spatial grid. The $n_s(\mathbf{r})$ so obtained can then be inserted back into eq 6 to obtain a refined estimate of $n(\mathbf{r})$. The cycle can thus be repeated over and over, iterating until convergence is obtained.

(32) This formula omits some additional terms involving integrals of the potential $-2a[\bar{n}(\mathbf{r}) - \bar{n}_s(\mathbf{r})]$ that are small both in the limit of very small and very large excluded volume regions.
(33) Narten, A. H.; Levy, D. *J. Chem. Phys.* **1971**, *55*, 2263.
(34) Eisenberg, D.; McLachlan, A. D. *Nature* **1986**, *319*, 199.
(35) Juffer, A. H.; Eisenhaber, F.; Hubbard, S. J.; Walther, D.; Argos, P. *Protein Sci.* **1995**, *4*, 2499.
(36) Vallone, B.; Miele, A. E.; Vecchini, P.; Chiancone, E.; Brunori, M. *Proc. Natl. Acad. Sci. U.S.A.* **1998**, *95*, 6103.
(37) Pratt, L. R.; Pohorille, A. *Proc. Natl. Acad. Sci. U.S.A.* **1992**, *89*, 2995.
(38) Lum, K.; Chandler, D. *Int. J. Thermophys.* **1998**, *19*, 845.
(39) Branden, C.; Tooze, J. *Introduction to Protein Structure*; Garland Publishing: New York, 1991.
(40) Munson, M.; Anderson, K. S.; Regan, L. *Folding Des.* **1997**, *2*, 77.
(41) Lum, K. Ph. D. Thesis, University of California, Berkeley, 1998.